Structure, Mechanics and Failure of Stochastic Fibrous Networks: Part II—Network Simulations and Application

C. W. Wang

A. M. Sastry

Department of Mechanical Engineering and Applied Mechanics, The University of Michigan, Ann Arbor, MI 48109-2125

Applications for porous fibrous materials range from electrochemical substrates to web reinforcement in polymeric composite materials. The details of local load transfer are studied in a class of cost-effective, stochastic fibrous networks used in battery applications. The connectivity of these materials is quantitatively related to modulus and strength, and detailed results of different simulations approaches in approximating material construction are discussed. In Part II, we focus on the consequences of various microscale assumptions concerning bonding, beam type, failure mode and simulation scale on effective moduli and peak loads. We show that the effects of scale are important even in a tight range of window sizes (one-tenth to ten times the staple length), especially as compared to the relative insensitivity of conductivity to scale, when only bulk conduction is considered. We also discuss issues of connectivity at the scale of the porous material rather than element-by-element. This work points toward use of simple constructions to model complex behavior, and may ultimately provide insight into modeling of a large class of porous materials. [S0094-4289(00)01604-2]

1 Introduction

In our previous work in modeling the mechanical and transport properties of NiMH battery substrates, we uncovered a few critical theoretical and practical issues in simulations. Several groups have recently adopted the strategy of attempting to solve a more general stochastic problem in pursuit of understanding more generally the importance of scale in numerical simulation of linear problems [1,2]. Here, as a continuation of our previous work, we investigate the mechanics and transport properties for a single class of materials, with simulations tightly coupled with validating experiments. We find significant differences in scale effects in simulation of transport properties [3] and mechanics properties [4]. Essentially, we have found that solution of a single set of coupled partial differential equations for heterogeneous domains is insufficient to model the different mechanisms involved in the separate physical processes of conduction and mechanical load sharing. Moreover, while conduction processes in high-contrast networks can often be modeled quite accurately by considering only microstructure (i.e., for bulk conduction processes), mechanics simulations require detailed consideration of microscale mechanisms of load transfer and failure.

Indeed, networks even with only linear elastic elements produce rich and physically accurate behavior if reasonable local failure criteria are applied. We expect that our strategy in constructing simple networks to model real materials' behavior will be rather directly extended to other scales of consideration, including the nanoscale, simply because of the preponderance of materials (including molecules) that can be viewed, at some degree of deformation, as linear elastic. Certainly, investigation of the effects of basic changes in the simple load transfer mechanisms investigated here is needed in order to reasonably address the effect of material constitutive nonlinearity.

The materials modeled in the present studies are porous substrates for NiMH positive electrodes. Several key battery technologies are presently limited by materials selection and design. Two promising technologies, NiMH and Li-ion, both rely on fiber/particle blends in the substrate materials of their electrodes to provide mechanical stiffness and strength, and assure good conductivity of the plates. Previous work on percolation and conductivity of similarly constructed (theoretical) networks include classic work in percolation [5], and work on the mechanics of nonwovens [6–12]. The present authors have developed a set of techniques to model porous, fibrous materials at the microscale, incorporating the microstructure directly in the simulations. These techniques have been validated with experimental data, including mechanical tests, conductivity measurements, and battery tests [3,4,13–17]. While these techniques have offered a validated means of analysis of NiMH positive plate substrates, including simulation of the effects of electrodeposition phenomena on mechanical and transport properties, here we focus on quantifying the effect of selection of specific micromechanics assumptions on somewhat more generalized network response.

In Part I of this work [18], we showed closeness in stiffnesses of two-beam arrays for Euler-Bernoulli and Timoshenko beam assumptions; the maximum stresses predicted by these beam types were similarly close. We further described three techniques for modeling fiber-fiber joints (rigid bond, torsion spring, and compliant zone) demonstrating equivalence of the more physically realistic compliant zone model with the torsion spring model described previously.

Here, we present results of network-scale simulations. We identify features of network which allow sometimes very simplifying assumptions to be made (e.g., selection of Euler-Bernoulli beams over Timoshenko beams). We also describe features to which network response is highly sensitive, for instance, selection of conditions for placement of "joints" in a network comprised of staple fibers where separation of the segments as independent elements drastically alters mechanical properties. Reiterating our objectives from Part I, we aim

1 to assess the effect of choice of beam types in models for fibers, and the effect of assumptions at fiber-fiber bonds, on the simulated overall network response;

2 to examine the effect of assumptions regarding material connectivity on the simulated overall network response;

3 to examine the effects of scale in simulation, especially regarding strength and damage tolerance; and

Contributed by the Materials Division for publication in the JOURNAL OF ENGINEERING MATERIALS AND TECHNOLOGY. Manuscript received by the Materials Division May 26, 2000; revised manuscript received May 30, 2000. Guest Editor: Assimina Pelegri.

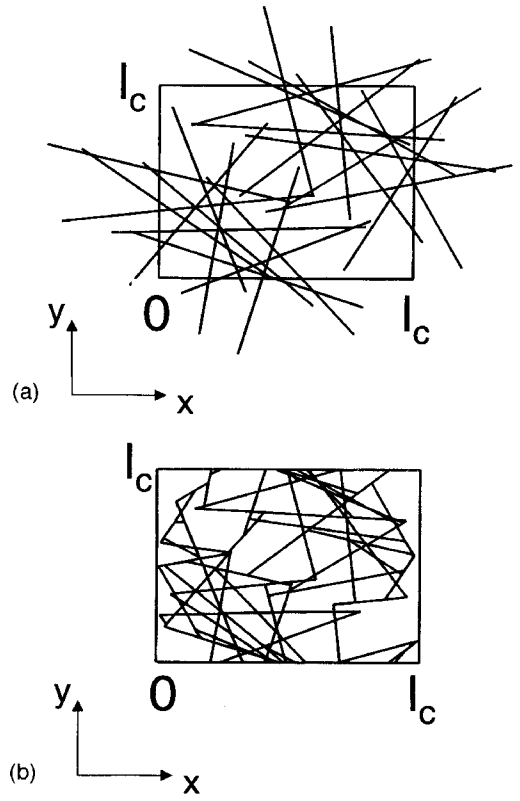

Fig. 1 Original (*a*) and reduced (*b*) networks, based on elimination of nonload-bearing structures for unidirectional (*y*-direction) loading only. Calculated parameters on the network as generated are as follows: original volume fraction −20 percent, reduced volume fraction −16 percent, number of intersection points −216; number of segments −361; average segment length −0.053; standard deviation, segment length −0.054. The fibers are randomly placed, and have aspect ratio $l/d=100$, with uniform staple length $l=1$, with length of cell $l_c=1$.

4 to assess the ability of spring-jointed models in predicting real materials response, as compared to a class of fiber-particle networks.

In Part II, the present paper, we address the final two points, examining both real versus simulated response of NiMH substrates, and scale effects in simulations as they affect predictions of properties.

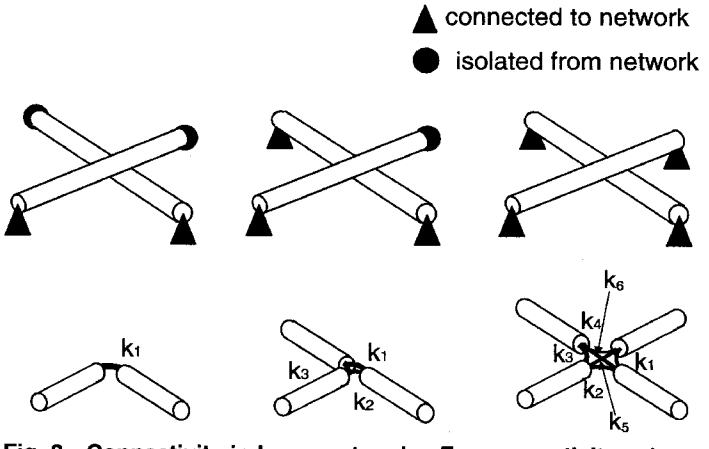

Fig. 2 Connectivity in beam networks. For connectivity calculated via a 2D assumption for beams, only three cases arise, practically speaking, wherein (i) two, (ii) three, or (iii) four beams, respectively, intersect at a single point.

2 Network Simulations: Effects of Microscale Assumptions

Networks generated as described earlier share the following features: 1) each realization has different final (reduced) volume or mass fraction than originally imposed on the unit cell, 2) a variety of interior structures arise in networks, but they are largely untriangulated, and thus almost invariably statically indeterminate, 3) each realization has unique connectivity. The calculated parameters on the network of Figs. 1, for example, are as follows: original volume fraction −20 percent, reduced volume fraction −16 percent, number of intersection points −216; number of segments −361; average segment length −0.053; standard deviation,

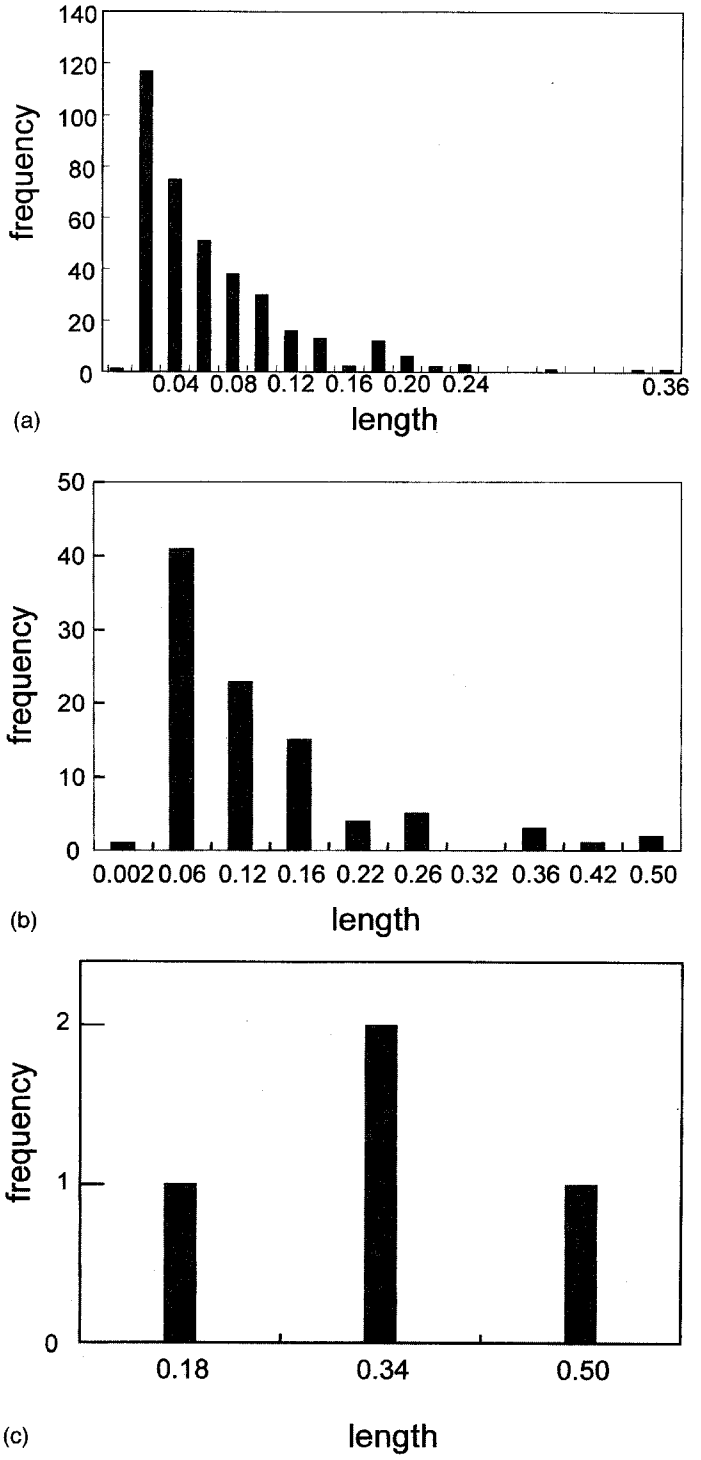

Fig. 3 Frequency distribution plots for segment size, for three aspect ratios of fibers, (*a*) $l/d=100$, (*b*) $l/d=50$ and (*c*) $l/d=10$

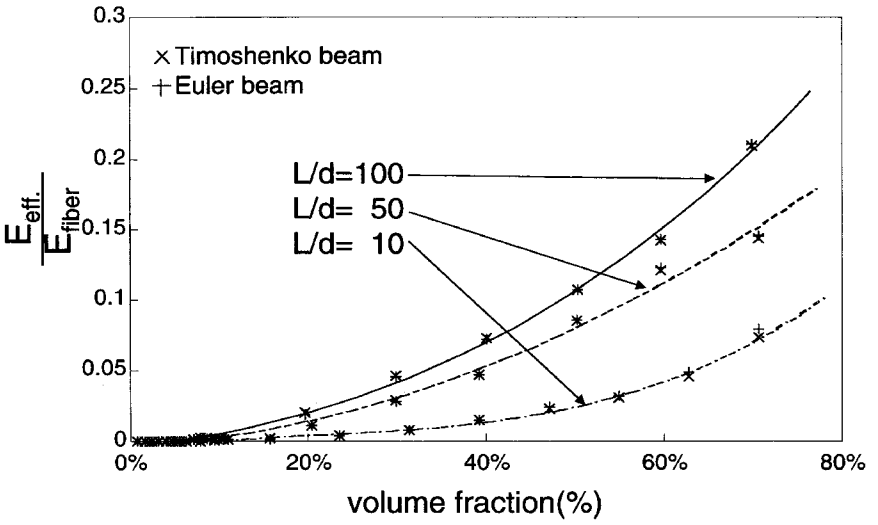

Fig. 4 Comparison of the Euler-Bernoulli beams and Timoshenko beams in simulations of effective network modulus, for a range of volume fractions and three aspect ratios (100,50,10). For all cases, $l/l_c=1$.

segment length −0.054. The fibers are randomly placed, and have aspect ratio $l/d=100$, with uniform staple length $l=1$, with length of cell $l_c=1$. Thus, a small number of initial parameters specifying the type of network produces stochastic structures of highly variable and complex interior structure.

For 1D fibers, there are only three practically-arising types of fiber junctures, as shown in Fig. 2. Reduction of extraneous ends in the network for purpose of efficient analysis results in junctures of 2, 3, or 4 segments, since not more than two individual fibers overlap at a single point. With low aspect ratio, this assumption of course breaks down, since the fiber thickness must be considered in order to model connectivity.

Fiber length between joints in the network is a critical factor in response of the network; in the current approach, this information is used explicitly rather than as an average value. As shown in the frequency distribution plots of Fig. 3, resulting segment lengths depend heavily upon the geometry of the constituent staple fibers. The scale of the simulation relative to the material scale is also important. At a very small scale, no bonds between fibers might arise in the simulated area. The effective modulus in such cases would be higher, since load would be borne disproportionately by tension and bending in single continuous fibers, instead of primarily by jointed, more compliant assemblies.

We first examine the effects of three sets of critical assumptions as they affect network response: beam type, local failure criterion, connectivity and definition of the element, and scale of simulation.

2.1 Element Models: Effects of Transverse Shear. Use of more accurate beam elements in modeling networks was explored at the microscale in Part I of this work. Significant differences in calculated loads and displacements were found only for very low aspect ratio segments in Euler-Bernoulli versus Timoshenko beams. However, even in cases of very low aspect ratio, producing segments of short length (per the examples of Fig. 3, with a set of network results shown for a low aspect ratio of 10), we find little difference in the Euler-Bernoulli and Timoshenko beam networks (Fig. 4, for a "window size," or length of representative cell, of $l_c=1$). Thus, the network results show less sensitivity to the selection of element type than the simpler cases investigated at the microscale. This insensitivity is due to the function of short segments in these networks. Primarily, network deformation is

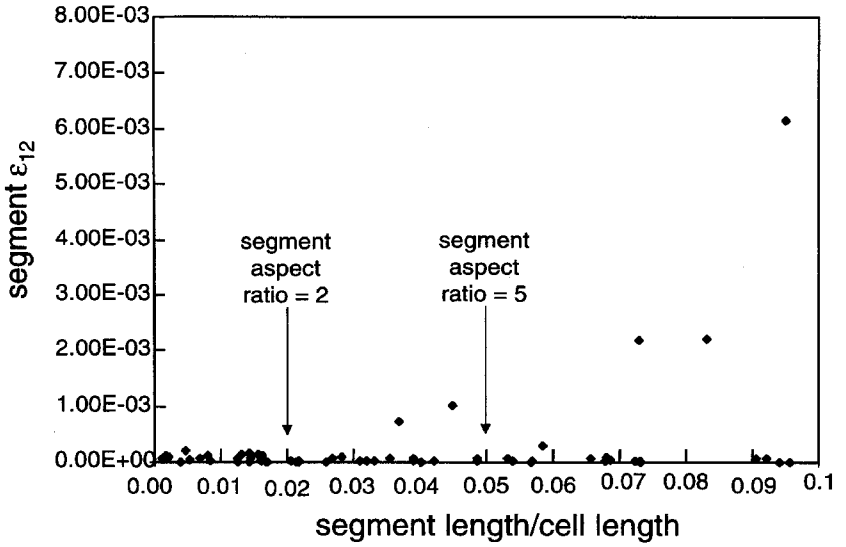

Fig. 5 Comparison of segment strain versus normalized segment length in a single network with $l/d=100$, $l/l_u=1$, and original volume fraction of 10 percent

concentrated in longer lengths of fibers. Figure 5 shows a comparison of segment length to shear strain in the element, for a sample simulation with $l/d=100$, $l/l_u=1$, and original volume fraction of 10 percent. Overall, we observed that the very shortest segments are "clustered" and essentially function as rigid interconnects for fewer, longer fibers in networks. Thus, it seems unlikely that improvements in modeling stresses at smaller than the beam scale would provide much insight for large fiber networks.

2.2 Failure Criteria and Network Damage Tolerance. Maximum stresses in assemblies of connected beams necessarily occur at the nodes. Two local strength-of-materials failure criteria are conceivable, representing the extremes of nodal damage tolerance; these are illustrated in Figs. 6. For maximum stress occuring at node *b* (Fig. 6(*a*)) one could fail only the beam at which stress is maximized, i.e., segment 2 (Fig. 6(*b*)), or, more conservatively, remove the entire node (Fig. 6(*c*)).

Simulations of real networks (with geometries similar to those of NiMH battery materials) show little sensitivity to the choice of beam or nodal failure, in terms of prediction of peak stress (with real network behavior shown in the schematic of Fig. 7(*a*)). Figures 7(*b*) and 7(*c*) illustrate, for three aspect ratios (100, 50, 10), $l/l_c=1$, and for both Euler-Bernoulli and Timoshenko beams. Thus, we suggest use of the simpler nodal failure criterion, as these are less computationally intensive, i.e., remove portions of the network from the simulation more quickly.

2.3 Segments Versus Staple Fibers as Elemental Units. Composition of fiber-fiber interconnects are highly variable, per examination of micrographs of NiMH materials, and recently, Li-ion battery materials. In generation of networks, we may view overlapping staple fibers as producing separate segments for analysis, as shown in Fig. 2 (resulting in 6 independent torsion springs if such a joint assumption is used), or we may preserve the fibers as the elemental units, joining continuous fibers with single torsion springs, as shown in Fig. 8. Preservation of the staple fiber as the elemental unit has the effect of increasing the overall stiffness, and also affects the scale-dependence of simulations. While this method is closer to stated physical model of real materials wherein straight fibers are used and bonded, actual materials often contain many kinked or curved fibers. Thus, we expect a simple model to fall somewhere between the assumptions of Fig. 2 and Fig. 8.

2.4 Scale Effects in Simulation: Mechanics Versus Transport Properties. We illustrate the importance of scale in simulation with a simple example—a zig-zag arrangement of segments, as shown in Fig. 9. For a range of ratios of staple length in simulation to simulated lengthscale, and torsion spring constants, we present solutions for effective modulus and maximum stress in the simple network via a dummy load method. Sample derivations follow. By equilibrium considerations, we calculate the axial force inside each beam, the transverse force inside each beam, and the moment. For two beams, 1 and 2, we have the axial forces and transverse forces and moments,

Beam 1.

$$\begin{aligned} S_1 &= F_x\cos\gamma - F_y\sin\gamma \\ T_1 &= F_x\sin\gamma + F_y\cos\gamma \\ M_1 &= -M - F_x\xi\sin\gamma - F_y\xi\cos\gamma \end{aligned} \tag{1}$$

Beam 2.

$$\begin{aligned} S_2 &= F_x\cos\gamma + F_y\sin\gamma \\ T_2 &= -F_x\sin\gamma + F_y\cos\gamma \\ M_2 &= -M - F_x(l\sin\gamma - \xi\sin\gamma) - F_y(l\cos\gamma + \xi\cos\gamma) \end{aligned} \tag{2}$$

For multiple beams, only M_i is altered. The potential energy becomes

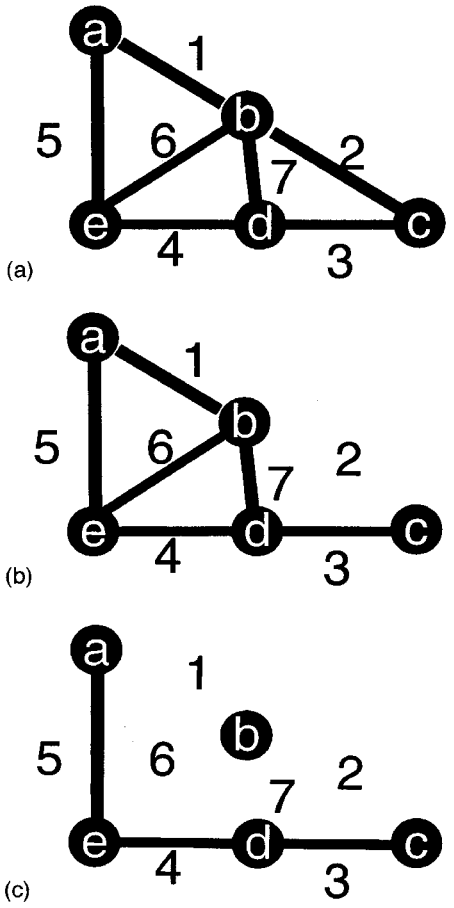

Fig. 6 Schematic of network failure criteria. The microstructure in (*a*), comprised of 7 fiber segments and 5 nodes, is deformed until a local failure initiates at node *b*. The least conservative failure progression assumption (*b*), the beam assumption, removes only fiber segment 2, since stress is maximized theoretically at its end at point *b*. The most conservative assumption, the node assumption, is shown in (*c*), wherein the entire node *b* fails, resulting in loss of beam segments 1, 2, 6, and 7.

$$U=\int_0^l\left(\frac{S_1^2}{2EA}+\frac{M_1^2}{2EI}\right)d\xi_1+\int_0^l\left(\frac{S_2^2}{2EA}+\frac{M_2^2}{2EI}\right)d\xi_2 \tag{3}$$

We obtain the displacement in each direction at the boundary edge as

$$\begin{aligned} dx &= \frac{\partial U}{\partial F_x} \\ dy &= \frac{\partial U}{\partial F_y} \\ d\phi &= \frac{\partial U}{\partial M} \end{aligned} \tag{4}$$

We restrict displacement on the right-hand side to the x-direction, so that $dy=d\phi=0$. Imposing $dx=X$, we obtain three equations and three unknowns: F_x, F_y, and M in terms of X. Per our definition of effective modulus, as

$$\frac{E_{\text{effective}}}{E_{\text{fiber}}}=\frac{F}{XAE_{\text{fiber}}} \tag{5}$$

we obtain the following expressions for cases (i), (ii), and (iii) of Fig. 9, as

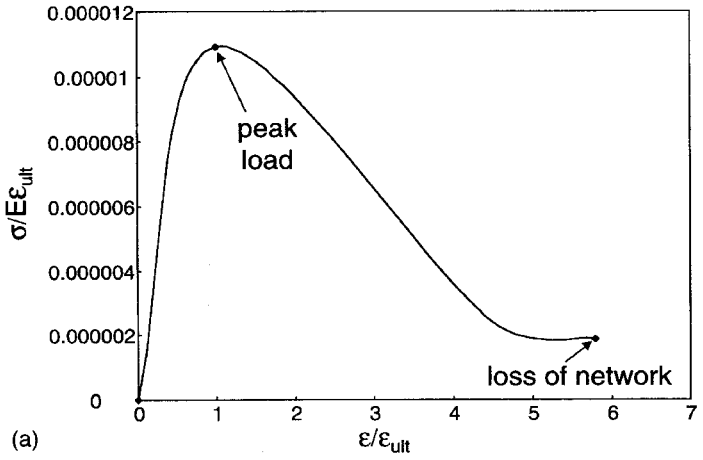

(a)

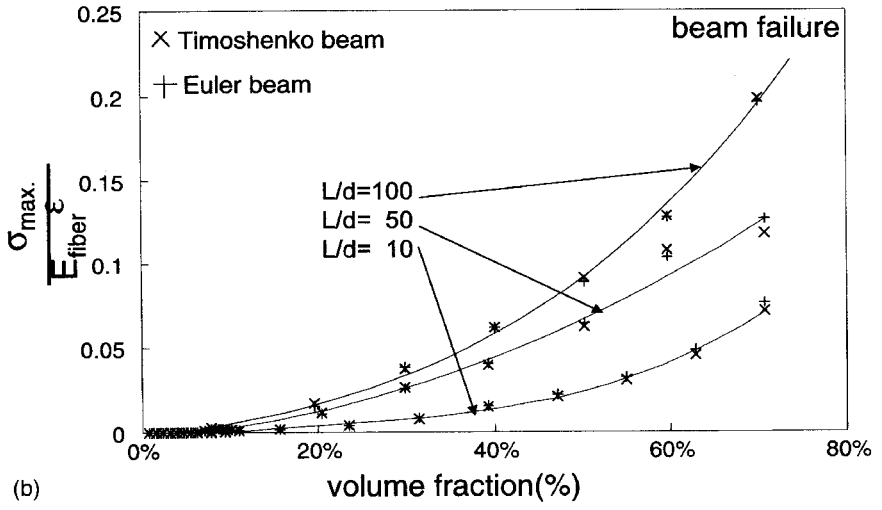

(b)

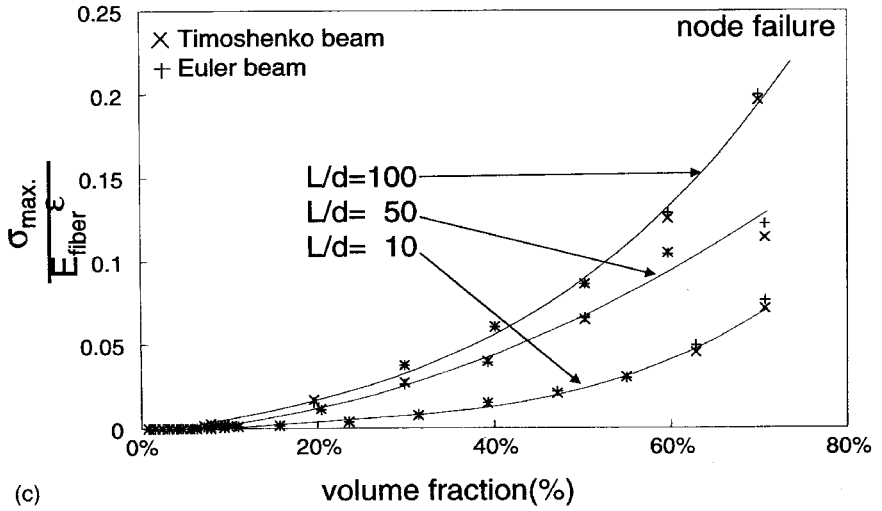

(c)

Fig. 7 Comparison of failure assumptions in predicting peak stress, with peak stress shown in the typical network stress-strain curve shown in (*a*). Peak stresses are shown for both Euler-Bernoulli and Timoshenko beam assumptions in (*b*), for a range of volume fractions and three aspect ratios (100,50,10). For all cases, $l/l_c=1$.

case (i):

$$\frac{E_{\text{effective}}}{E_{\text{fiber}}}=3\,\frac{I(2lK+EI)}{l(l^3AK\sin^2\gamma+6EI^2\cos^2\gamma+12lIK-12lIK\sin^2\gamma+2l^2EIA\sin^2\gamma)} \tag{6}$$

case (ii):

$$\frac{E_{\text{effective}}}{E_{\text{fiber}}}=\frac{3}{2}\,\frac{IK(4lK+3EI)}{l(2l^3K^2A\sin^2\gamma+24K^2Il\cos^2\gamma+6l^2KEIA\sin^2\gamma+18EI^2K\cos^2\gamma+3E^2I^2Al\sin^2\gamma)} \tag{7}$$

case (iii):

$$\frac{E_{\text{effective}}}{E_{\text{fiber}}} = \frac{IK(6lK+5EI)}{l(30EI^2K\cos^2\gamma+36lK^2I\cos^2\gamma+3l^3K^2A\sin^2\gamma+10l^2KEIA\sin^2\gamma+6E^2I^2l\sin^2\gamma)} \tag{8}$$

For $l=1/2$, 1/4 and 1/6, respectively for cases (i), (ii), and (iii). We find by substitution, case (i):

$$\frac{E_{\text{effective}}}{E_{\text{fiber}}} = 48\frac{I(K+EI)}{(AK\sin^2\gamma+48EI^2\cos^2\gamma+48IK\cos^2\gamma+4EIA\sin^2\gamma)} \tag{9}$$

case (ii):

$$\frac{E_{\text{effective}}}{E_{\text{fiber}}} = \frac{192\cdot IK(K+3EI)}{(K^2A\sin^2\gamma192K^2I\cos^2\gamma+12KEIA\sin^2\gamma+576EI^2K\cos^2\gamma+24E^2I^2A\sin^2\gamma)} \tag{10}$$

case (iii):

$$\frac{E_{\text{effective}}}{E_{\text{fiber}}} = \frac{432\cdot IK(K+5EI)}{(2160EI^2K\cos^2\gamma+432K^2I\cos^2\gamma+K^2A\sin^2\gamma+20KEIA\sin^2\gamma+72E^2I^2A\sin^2\gamma)} \tag{11}$$

which become, for $K\to 0$ (i.e., rigid bond)
case (i):

$$\frac{E_{\text{effective}}}{E_{\text{fiber}}} = 48\frac{I}{A\sin^2\gamma+48I\cos^2\gamma} \tag{12}$$

case (ii):

$$\frac{E_{\text{effective}}}{E_{\text{fiber}}} = 192\frac{I}{A\sin^2\gamma+192I\cos^2\gamma} \tag{13}$$

case (iii):

$$\frac{E_{\text{effective}}}{E_{\text{fiber}}} = 432\frac{I}{A\sin^2\gamma+432I\cos^2\gamma} \tag{14}$$

From (7) or (8) we confirm in the limit as $l\to 0$ (i.e., the beam is comprised of an infinite series of rigid bonds) that the $E_{\text{effective}}\to\infty$. Results for these cases are shown in Figs. 10(*a*) and 10(*b*). The clamped end condition in the derivation results in stiffer behavior in the two-beam arrays for low torsion constants, but a transition occurs at normalized torsion spring constants of 1. Above those values, there is a clear stiffness advantage to having fewer segments. This in turn clearly illustrates the effect of scale in mechanics simulations on jointed networks: window size, or scale of simulation (where here, the edge length is designated at l_c as in Part I of this work), strongly affects calculated mechanical properties.

This is not the case in calculation of transport properties for high contrast materials. Previously, it was shown [3] that for simulation scales one-tenth to equal the staple fiber length, little difference in calculated conductivity was found. Essentially, the increased length of fiber in even a zig-zag array alters only the total conductive volume, but does not alter the conduction mechanism if bulk conduction is considered. This clearly illustrates the difference in scale selection for simulations in separate physical processes, and the importance of experimental validation. In the materials studied by the present authors, models employing only bulk conduction fit the materials' conductivities quite well; in cases where surface conduction would be required, more analysis and simulation would be necessary to determine appropriate scales of simulation for transport.

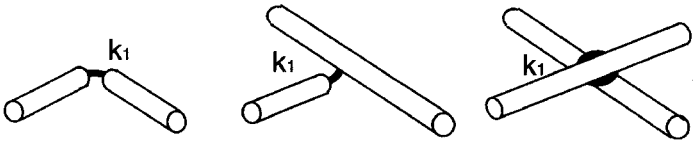

Fig. 8 Schematic of torsion springs at a fiber-fiber "joint" wherein staple fibers are preserved as an elemental unit rather than segments (as shown in Fig. 2). Only connections between segments from *different* fibers are modeled with torsion spring connections.

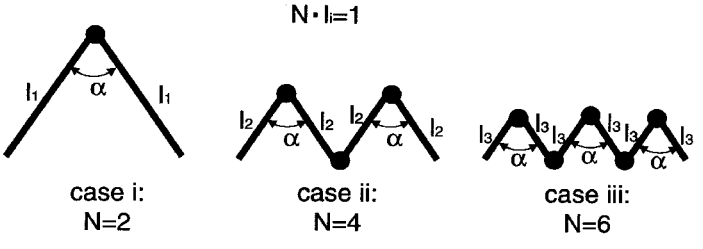

Fig. 9 Connectivity versus effective modulus in simple bilinear networks. Schematics of the illustrative cases are shown wherein segments (whose lengths sum to 1) are joined by torsion springs of variable stiffness.

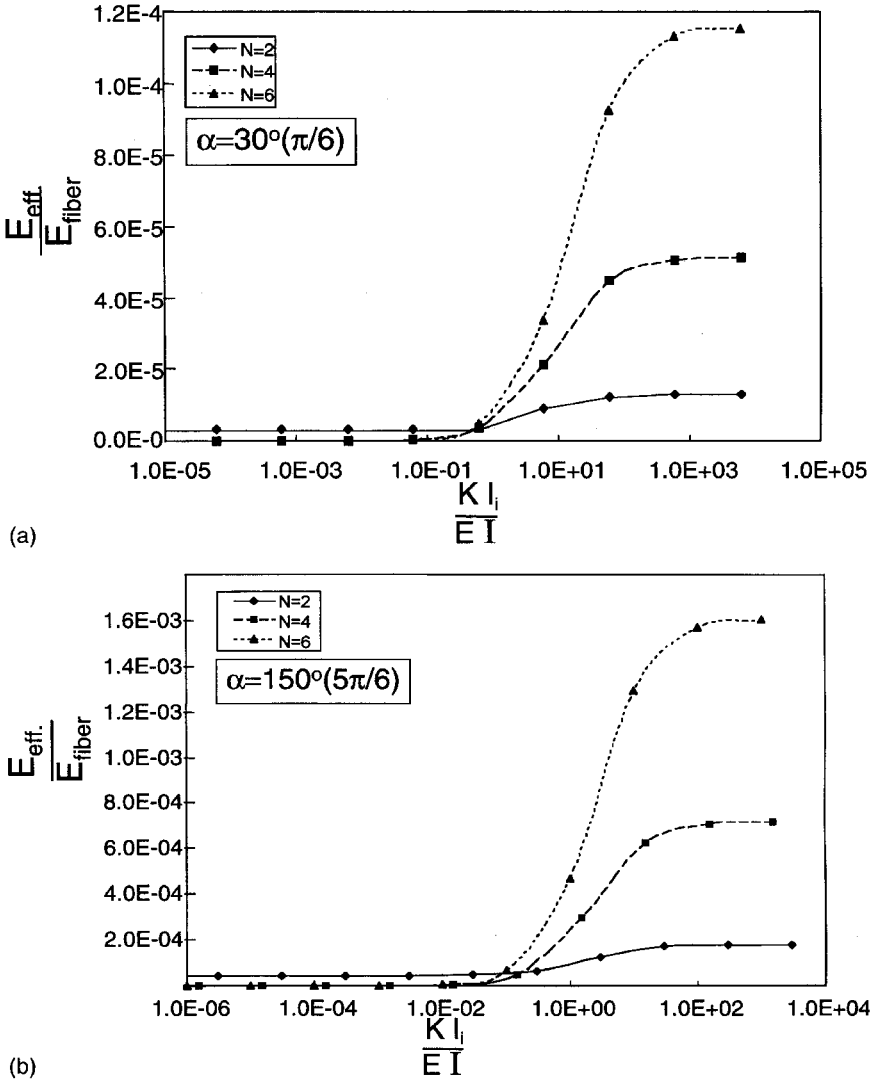

Fig. 10 Effective moduli (*a*) and maximum stresses (*b*) are given for α=30 and α=150 deg, for a range of torsion spring constants and a variable number of segments for arrays as shown in Fig. 9

3 Discussion: Connectivity, Scale and Effects on Modulus and Peak Stress

Microscale considerations affect network response profoundly, and though it may be possible to bound results via purely statistical approaches, it is important to distinguish between various scales and physical processes, such as mechanics and transport. The sometimes complex architectures seen in real materials can be efficiently simulated using only linear elastic elements, but some detail is required in imaging in order to make appropriate approximations of material properties. The intertwined effects of connection stiffness, segment or staple fiber length and scale had been reported previously [4,15]. Here we demonstrate the underlying theoretical reasons for these simulation results.

Figures 11 and 12 summarize some of the important findings here regarding scale, connectivity and their effect on network properties. The interrelationship of connectivity and scale are demonstrated by the results of Figs. 11, with normalized effective moduli (Fig. 11(*a*)) and peak stresses (Fig. 11(*b*)), for two normalized torsion spring constants. Staple fibers were of uniform aspect ratio of 10 in all cases. Because simulations were performed for representative cells slightly larger than the staple length (l_c=1.2), networks (of nonzero reduced volume fraction) consisted only of jointed beams. This scale effect is pronounced for a wide range of connector compliances, as shown for three different simulation sizes in Figs. 12(*a*) and (*b*).

Normalized effective moduli (Fig. 12(*a*)) and peak stresses (Fig. 12(*b*)), are shown for three normalized torsion spring constants, and for three representative cell sizes (l_c=0.5, 1.0, 10). Plots were for networks comprised of fibers with uniform aspect ratio of 100. Table 1 gives the values of moduli and peak stresses for all cases. The reduction in both modulus and strength are more dramatic for compliant, rather than stiff bonds, as scale of simulation size increases, in all cases. For the range of simulation sizes studied, there were no plateaux in these values, suggesting that unlike the conductivity problem, the mechanics problem requires a statistical approach detailed enough to quantify bond effects. For rigid bonds, the effect on moduli and strengths over three orders of magnitude of simulation lengthscale were moderately small; few networks studied, however, appeared from image analysis to contain well-defined fiber-fiber bonds. These results suggest that for multiphase networks, the statistics of connectivity of even unpercolated phases is warranted.

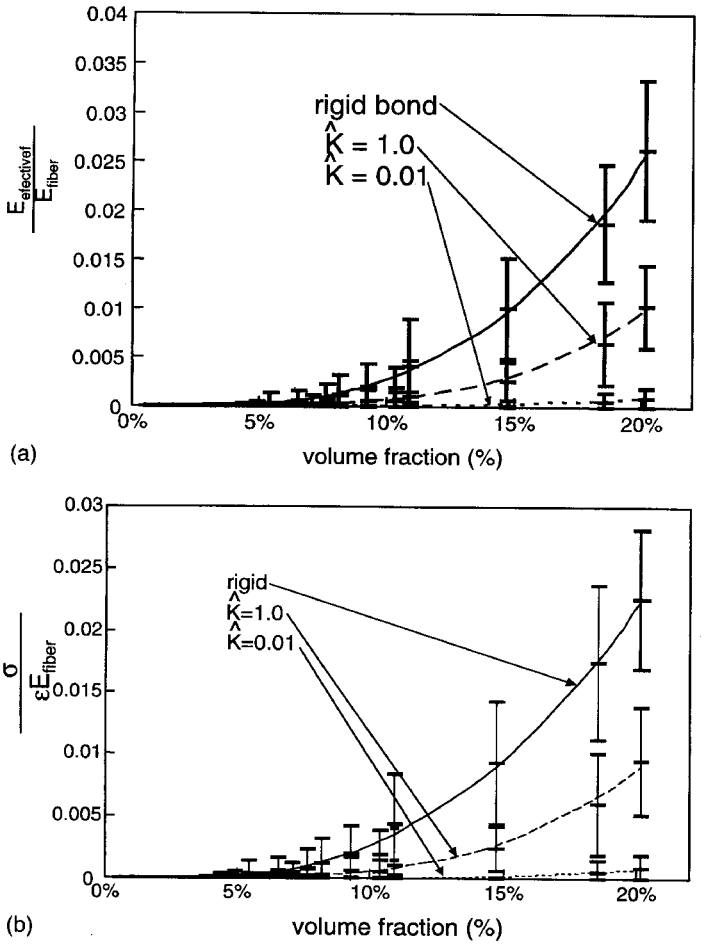

Fig. 11 Normalized effective moduli (*a*) and peak stresses (*b*), for two normalized torsion spring constants. Plots were for networks comprised of fibers with uniform aspect ratio of 10, with representative cell edge length of $l_c = 1.2$.

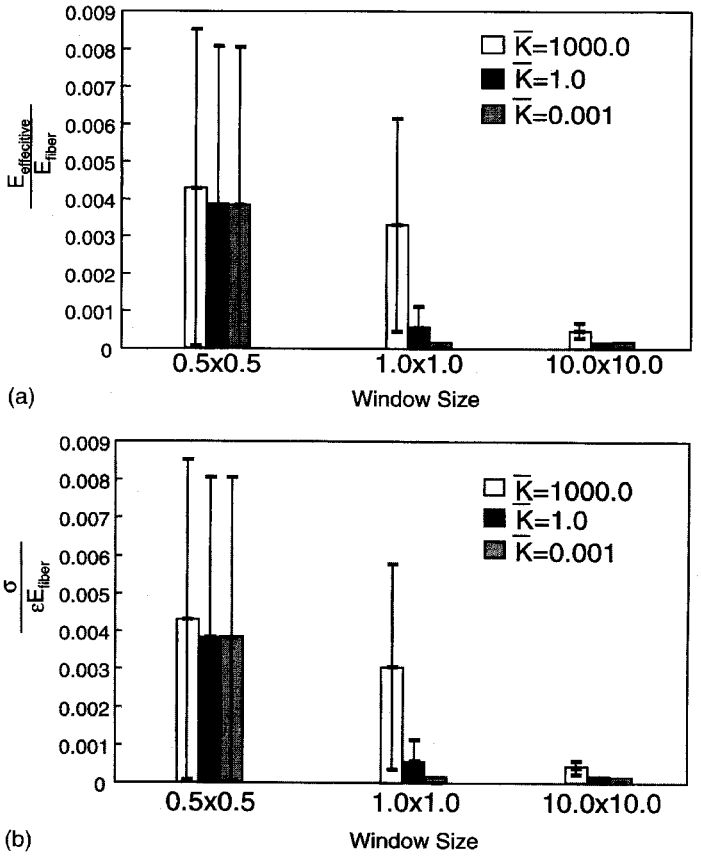

Fig. 12 Normalized effective moduli (*a*) and peak stresses (*b*), for three normalized torsion spring constants, and for three representative cell sizes ($l_c = 0.5, 1.0, 10$). Plots were for networks comprised of fibers with uniform aspect ratio of 100.

Table 1 Values for moduli and peak stresses shown in Figs. 12(*a*) and 12(*b*)

	l_c=0.5			l_c=1.0			l_c=10.0		
	K=1000	K=1.0	K=0.001	K=1000	K=1.0	K=0.001	K=1000	K=1.0	K=0.001
$\frac{E_{effective}}{E_{fiber}}$	4.290E-03	3.840E-03	3.822E-03	3.291E-03	5.569E-04	3.216E-06	4.846E-04	5.36E-05	8.02E-08
$\frac{\sigma}{\varepsilon E_{fiber}}$	4.290E-03	3.844E-03	3.822E-03	3.067E-03	5.489E-04	3.203E-06	4.082E-03	4.52E-05	5.80E-08

4 Conclusions/Future Work

We have shown that greater detail in beam modeling is probably unnecessary in these materials, but that the issue of scale is a complex one, especially when coupled with considerations of joint type. Simulations to determine peak load are relatively insensitive to local (total node versus beam) failure criteria; this may guide purely statistical efforts in modeling load sharing in damaged spring networks. The reality is, of course, somewhat more complicated, since many technologically important materials are comprised of multiple phases of different morphology, and connectivity is seldom well-described by a single connection point.

Future work will focus on greater detail in connectivity, including investigation of 3D loads in fibers near the intersection point. While the 2D approaches presented here have allowed focus on critical network specifics, including connectivity, scale of simulation, and bond type, the connectivity of 3D networks requires understanding of how a nonpercolated phase might act to join a percolated one, as occurs frequently in this class of materials.

Acknowledgments

The authors gratefully acknowledge support from our sponsors, including a National Science Foundation PECASE award, contracts provided by the U.S. Department of Energy, through the Exploratory Technology Program of the Lawrence Berkeley Laboratories and funding from the U.S. Army Research Office. The authors also thank the reviewers for their carefulness and helpful comments.

References

[1] Ostoja-Starzewski, M., Sheng, P. Y., and Alzebdeh, K., 1996, "Spring Network Models in Elasticity and Fracture of Composites and Polycrystals," Comput. Mater. Sci., **7**, pp. 82–93.

[2] Drugan, W. J., and Willis, J. R., 1996, "A Micromechanics-Based Nonlocal Constitutive Equation and Estimates of Representative Volume Element Size for Elastic Composites," J. Mech. Phys. Solids, **44**, pp. 497–524.

[3] Cheng, X., and Sastry, A. M., 1999, "On Transport in Stochastic, Heterogeneous Fibrous Domains," Mech. Mater., **31**, pp. 765–786.

[4] Wang, C. W., Cheng, X., Sastry, A. M., and Choi, S. B., 1999, "Investigation

of Failure Processes in Porous Battery Substrates: Part I—Experimental Findings," ASME J. Eng. Mater. Technol., **121**, pp. 503–513.
[5] Kirkpatrick, S., 1973, "Percolation and conduction," Rev. Mod. Phys., **45**, No. 4, pp. 574–588.
[6] Niskanen, K., 1993, "Strength and Fracture of Paper," *Products of Papermaking: Transactions of the Tenth Fundamental Research Symposium*, Baker, C. F., ed., PIRA International, United Kingdom, Vol. 2, pp. 641–725.
[7] Backer, S., and Petterson, D. R., 1960, "Some Principles of Nonwoven Fabrics," Text. Res. J., **30**, pp. 704–711.
[8] Hearle, J. W. S., and Newton, A., 1968, "Part XV: The Application of the Fiber Network Theory," Text. Res. J., **1**, pp. 343–351.
[9] Hearle, J. W. S., 1980, "The mechanics of Dense Fibre Assemblies," *The Mechanics of Flexible Fibre Assemblies*, Hearle, J. W. S., Thwaites, J. J., and Amirbayat, J., eds., Sijthoff and Noordhoff, New York, pp. 51–86.
[10] Lu, W., Carlsson, L. A., and Andersson, Y., 1995, "Micro-Model of paper, Part 1: bounds on elastic properties," Tappi J., **78**, pp. 155–164.
[11] Lu, W., and Carlsson, L. A., 1996, "Micro-Model of paper, Part 2: statistical analysis of the paper structure," Tappi J., **79**, pp. 203–210.
[12] Lu, W., Carlsson, L. A., and de Ruvo, A., 1996, "Micro-Model of paper, Part 3: Mosaic model," Tappi J., **79**, pp. 197–205.
[13] Sastry, A. M., Choi, S. B., and Cheng, X., 1998, "Damage in Composite NiMH Positive Electrodes," ASME J. Eng. Mater. Technol., **120**, pp. 280–283.
[14] Sastry, A. M., Cheng, X., and Wang, C. W., 1998, "Mechanics of Stochastic Fibrous Networks," J. Thermopl. Compos. Mater., **30**, pp. 288–296.
[15] Cheng, X., Wang, C. W., Sastry, A. M., and Choi, S. B., 1999, "Investigation of Failure Processes in Porous Battery Substrates: Part II—Simulation Results and Comparisons," ASME J. Eng. Mater. Technol., **121**, pp. 514–523.
[16] Cheng, X., Sastry, A. M., and Layton, B. E., 2000, "Transport in Stochastic Fibrous Networks," ASME J. Eng. Mater. Technol., accepted.
[17] Cheng, X., Wang, C. W., Sastry, A. M., and Choi, S. B., 1999, "Investigation of Failure Processes in Porous Battery Substrates: Part II—Simulation Results and Comparisons," ASME J. Eng. Mater. Technol., **121**, pp. 514–523.
[18] Wang, C. W., Berhan, L., and Sastry, A. M., 2000, "Structure, Mechanics and Failure of Stochastic Fibrous Networks: Part I—Microscale Considerations," ASME J. Eng. Mater. Technol., **122**, pp. 450–459.